Geophysical Journal International

Geophys. J. Int. (2010) **180,** 623–634 doi: 10.1111/j.1365-246X.2009.04419.x

A new projection of sea level change in response to collapse of marine sectors of the Antarctic Ice Sheet

Natalya Gomez,[1] Jerry X. Mitrovica,[1] Mark E. Tamisiea[2] and Peter U. Clark[3]

[1] *Department of Earth and Planetary Sciences, Harvard University,* 20 *Oxford Street, Cambridge,* MA 02138*, USA. E-mail: ngomez@fas.harvard.edu*
[2] *Proudman Oceanographic Laboratory,* 6 *Brownlow St., Liverpool* L3 5DA*, United Kingdom*
[3] *Department of Geosciences, Oregon State University, Corvallis,* OR 97331*, USA*

Accepted 2009 October 12. Received 2009 October 8; in original form 2009 January 5

SUMMARY

We present gravitationally self-consistent predictions of sea level change that would follow the disappearance of either the West Antarctic Ice Sheet (WAIS) or marine sectors of the East Antarctic Ice Sheet (EAIS). Our predictions are based on a state-of-the-art pseudo-spectral sea level algorithm that incorporates deformational, gravitational and rotational effects on sea level, as well as the migration of shorelines due to both local sea-level variations and changes in the extent of marine-based ice cover. If we define the effective eustatic value (EEV) as the geographically uniform rise in sea level once all marine-based sectors have been filled with water, then we find that some locations can experience a sea level rise that is ∼40 per cent higher than the EEV. This enhancement is due to the migration of water away from the zone of melting in response to the loss of gravitational attraction towards the ice sheet (load self-attraction), the expulsion of water from marine areas as these regions rebound due to the unloading, and the feedback into sea level of a contemporaneous perturbation in Earth rotation. In the WAIS case, this peak enhancement is twice the value predicted in a previous projection that did not include expulsion of water from exposed marine-sectors of the West Antarctic or rotational feedback. The peak enhancements occur over the coasts of the United States and in the Indian Ocean in the WAIS melt scenario, and over the south Atlantic and northwest Pacific in the EAIS scenario. We conclude that accurate projections of the sea level hazard associated with ongoing global warming should be based on a theory that includes the complete suite of physical processes described above.

Key words: Sea level change; Earth rotation variations; Antarctica.

1 INTRODUCTION

As the Earth moves into a period of continued and potentially increased global-scale warming, questions regarding the stability of present-day ice reservoirs, including the polar ice caps and mountain glaciers, have become more pressing. The Antarctic ice sheet, with a volume that accounts for ∼90 per cent of all freshwater on the Earth's surface (3×10^{16} m^3), is a central focus of this interest, particularly because a large fraction rests on bedrock below sea level (Fig. 1). In this regard, most discussions of future instability are preoccupied with the possible collapse of the West Antarctic Ice Sheet (WAIS), which is separated from the East Antarctic Ice Sheet (EAIS) by the Transantarctic Mountains and the Ronne–Filchner Ice Shelf, and which is almost entirely characterized by a marine-based setting. However, large sectors of the EAIS, particularly in Wilkes Land (∼120–150°E) and in the vicinity of the Amery Ice Shelf and Lambert Glacier (∼70°E), have a base that also lies well below local sea level (Fig. 1) but the impact of their destabilization on sea level has not been previously addressed.

What would the change in sea level be as a consequence of the collapse of these marine-based sectors of the Antarctic Ice Sheet? It is somewhat surprising that the answer to this question has not yet been fully explored, and that values that are quoted within the literature—both mainstream and scientific—can vary widely depending on the level of scientific sophistication used to generate the estimates. For example, if one were to convert the grounded portion of the volume cited above into a volume of water, and then distribute this volume in a geographically uniform manner throughout the global oceans, then one would arrive at the so-called eustatic estimate of ∼70 m. If, however, one were to take into account the negative topography of the bedrock, which would presumably serve as accommodation space for meltwater, then the geographically uniform increase in sea level, which we will term the effective eustatic value (EEV), would be closer to 55–60 m. In regard to the WAIS, the analogous eustatic and EEV are ∼8 and ∼5 m, respectively. The latter is a widely cited estimate (Mercer 1978), and it is quoted, for example, in chapter 10 of the most recent assessment of the IPCC (2007).

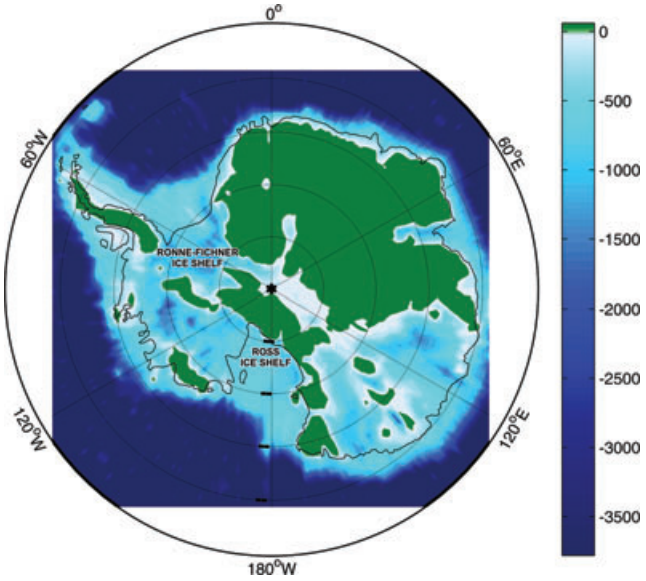

Figure 1. Map showing bedrock topography (in metres) over the Antarctic and vicinity. Contours are only shown over locations where this topography is less than zero in order to highlight the extent of marine-based settings.

However, it has been known for well over a century (Woodward 1888) that a rapidly melting ice sheet will produce a markedly non-uniform change in sea level. This spatial variability is largely driven by the self-attraction of the surface mass (ice plus ocean) load. Specifically, an ice sheet exerts a gravitational (tidal) attraction on the surrounding ocean, which leads to a build-up of water close to the ice mass. As the ice sheet melts, the integrated mass of the oceans will certainly increase; however, the tidal attraction will decrease, leading to a migration away from the zone of melting. Woodward (1888) showed, using a simple rigid (i.e. non-deforming) earth model, that the migration process will dominate within a region 2000 km from the ice sheet. In this 'near-field' zone, sea level will fall in response to the melting event, while it will rise by progressively larger values at greater distance. The predicted migration of water is accentuated in more recent studies, which include elastic deformation of the solid surface, since the near-field of the ice sheet will also be subject to crustal uplift which contributes to the sea level fall (Farrell & Clark 1976; Clark & Primus 1987; Nakiboglu & Lambeck 1991; Conrad & Hager 1997; Mitrovica *et al.* 2001; Tamisiea *et al.* 2001)

Since this geographic variability is due largely to load self-attraction, changes in the mass balance of a specific ice reservoir will produce a distinct pattern of sea level change. Hence these patterns have come to be known as sea level 'fingerprints' (Plag & Jüttner 2001). Mitrovica *et al.* (2001) showed that the geographic variation in secular trends evident in a widely distributed subset of 20th century tide gauge records can be explained by a weighted sum of fingerprints from melting of polar ice sheets and mountain glaciers. Their analysis, which demonstrated that such records could be used to constrain not only the amplitude of recent sea level rise but also the relative contributions from various sources, has motivated renewed interest in the physics of sea level change following rapid melting events. This interest has been further broadened by efforts to infer the source of sea level changes that have accompanied late Quaternary, ice-age climate events (Clark *et al.* 2002; Kendall *et al.* 2008).

Many of these recent studies have calculated sea level fingerprints associated with melting from the Antarctic Ice Sheet or a subregion, including the WAIS (Mitrovica *et al.* 2001; Tamisiea *et al.* 2001; Clark *et al.* 2002). However, to our knowledge, the first fingerprint of this kind was computed by Clark & Lingle (1977) who considered the impact of a future, uniform thinning of the WAIS on sea level. We reproduce their result in Fig. 2. The contours, as in the original publication, are normalized by the eustatic sea level change associated with the melting event.

As discussed above, melting from the WAIS leads to a sea level fall in the vicinity of this region, and an increase in the computed sea level rise as one moves towards the north. The mean sea level change is, of course, equal to 1, or the eustatic value. The maximum sea level rise is 20 per cent higher than the eustatic value in the north Atlantic and Indian Ocean and 26 per cent higher in the north Pacific. The pattern of sea level rise tends to taper towards the continental shelves, so that coastal sites experience a rise ∼10 per cent higher than the eustatic value. The broad scale pattern of water

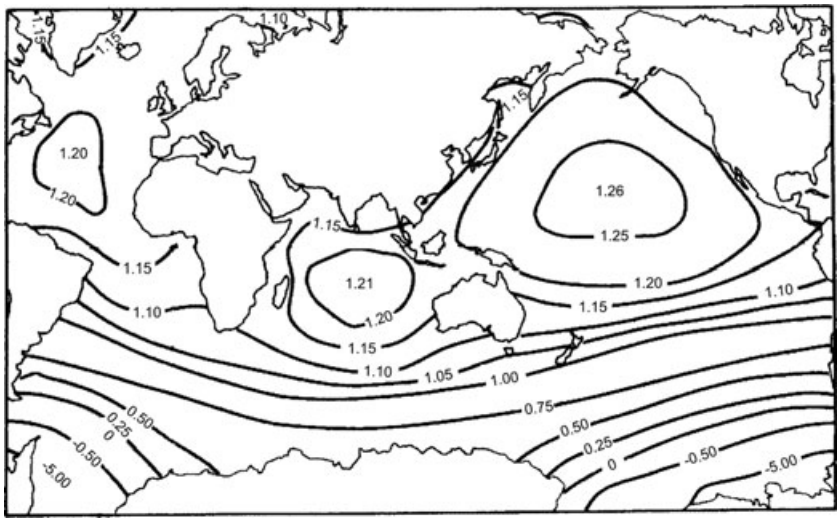

Figure 2. Sea level change, normalized by the eustatic sea level rise, in response to a uniform thinning of the West Antarctic ice sheet; the figure is reproduced, with minor modification, from Clark & Lingle (1977). As described in the text, Clark & Lingle (1977) applied a standard sea level theory valid for a non-rotating Earth in which all shorelines remain fixed with time. Thus, the prediction does not include inundation into, and expulsion out of, the West Antarctic or perturbations in sea level associated with changes in the Earth's rotation vector.

migration away from the WAIS is largely due, as we have discussed, to load self-attraction, while the tapering pattern over the northern oceans is due to loading effects. Specifically, the ocean load will tend to deform the crust of the elastic earth model downwards in the middle of the ocean and upwards over the (unloaded) continental regions.

Clark & Lingle (1977) argued that their calculation (Fig. 2) could be scaled to consider any uniform melting (or indeed growth) of the WAIS by multiplying the normalized prediction by the associated eustatic value (positive for melting and negative for growth). Since their calculations did not include the complete collapse of the WAIS, and specifically the inundation of the marine-based sectors of this ice sheet, one could treat the case of a full collapse by scaling the results in Fig. 2 by the EEV cited above (∼5 m).

It is unclear why the Clark & Lingle (1977) paper has been largely ignored in the subsequent discussions of projected sea level changes associated with a collapse of the WAIS, but this neglect was immediate (Mercer 1978) and sustained (e.g. IPCC 2007). In any event, the results in Fig. 2, and more recent studies by Mitrovica *et al.* (2001) and Clark *et al.* (2002), indicate that future sea level changes in response to loss of marine-based ice from Antarctica will neither be the eustatic nor the EEV, but rather a highly variable geographic signal that includes areas of sea level fall as well as zones of accentuated (relative to the EEV) sea level rise.

The Clark & Lingle (1977) analysis is not the final word on the issue, however, because it was based on a sea level theory (Farrell & Clark 1976) that makes two significant assumptions. First, the results in Fig. 2 do not include the feedback on sea level of contemporaneous perturbations in the Earth's rotation vector, a process that was included in more recent analyses of sea level fingerprints due to ongoing or late Quaternary melting events over the Antarctic (Mitrovica *et al.* 2001; Clark *et al.* 2002). Second, the calculation assumes that there is no marine-based ice, i.e. that the melting of the WAIS does not lead to inundation of parts of this sector. One might partially overcome this limitation by using the EEV, rather than the eustatic value, to scale the results in Fig. 2; however this ad-hoc correction misses an important piece of physics. In particular, the melting of the WAIS would also produce a rebound of the underlying crust, and this rebound will act to push water out of the region and into the global oceans. That is, the topographic hole that exists today below the WAIS is not the same as the hole that would exist after the melting initiates an immediate elastic rebound and a subsequent viscous uplift.

The sea level theory adopted by Clark & Lingle (1977) was a special (elastic) case of a theory that was developed to model sea level changes associated with the Late Pleistocene ice-age cycles (Farrell & Clark 1976). However, over the last decade this "standard" theory has been extended to include rotational feedback (e.g. Milne & Mitrovica 1996, 1998; Peltier 1998; Mitrovica *et al.* 2005) and shoreline migration due to local changes in sea level at coastlines and/or the growth or ablation of grounded marine-based ice (e.g. Johnston 1993; Milne 1998; Milne *et al.* 1999; Mitrovica & Milne 2003; Mitrovica 2003; Kendall *et al.* 2005). In this paper, we update and extend the Clark & Lingle (1977) results by adapting recent advances in ice-age sea level physics to compute and interpret fingerprints associated with melting from both the WAIS and marine-based sectors of the EAIS. The fingerprint for WAIS collapse was published, with few details, as a short note in Mitrovica *et al.* (2009); a similar study of the WAIS collapse was also performed by Bamber *et al.* (2009). Our goal here is to provide a far more comprehensive and state-of-the-art answer to the question posed throughout this introduction—what is the projected sea level change that would occur after the collapse of (parts of) the Antarctic Ice Sheet?

In the next section, we review in largely symbolic notation the theory and algorithm we apply to generate our sea level predictions. The theory is a summary of a derivation that may be found in the recent literature of ice-age sea level (Mitrovica & Milne 2003; Kendall *et al.* 2005), but we do not include it merely for completeness. Rather, as we discuss in formulating our numerical algorithm, the implementation of the theory necessary to predict future sea level changes is fundamentally different from the implementation one would use to calculate ice-age sea level variations. The difference arises because the initial (i.e. before loading) topography is known in the former case, but it is unknown in the latter application.

2 A REVISED THEORY FOR PROJECTIONS OF FUTURE SEA LEVEL CHANGE

Mitrovica & Milne (2003) and Kendall *et al.* (2005) derived a generalized sea level theory for application to problems in glacial isostatic adjustment (GIA). Furthermore, they outlined a suite of numerical algorithms tailored to the ice-age problem; in particular, these algorithms were designed for a system that evolves from the onset of ice-age loading, at some time in the past, up to the present-day. In this section we briefly review this generalized theory, and we derive a revised numerical algorithm suitable for calculations that yield projections of future sea level change.

We begin by denoting the radial position of the sea surface and solid surface, where the latter does not include ice height, as G and R, respectively. The former symbol is commonly adopted with the GIA literature because the position of the sea surface is taken to be identical, within the static sea level theory, to the position of the gravitational equipotential referred to as the geoid. The fields G and R may be defined globally, and their difference yields sea level

$$SL(\theta, \psi, t_j) = G(\theta, \psi, t_j) - R(\theta, \psi, t_j). \tag{1}$$

where θ and ψ denote the colatitude and east-longitude, and t_j is the time. With this definition, a simple relationship holds between topography (not including ice height) and sea level

$$T(\theta, \psi, t_j) = -SL(\theta, \psi, t_j). \tag{2}$$

Our definition of topography and the radial position of the solid surface can easily be altered to include the ice height. However, we have chosen to proceed in the above manner in order to be consistent with the previous literature. Moreover, this definition simplifies the connection between topography and various concepts related to sea level. For example, locations with positive topography (negative sea level) are synonymous with 'land', while marine settings are defined by negative topography (or positive sea level). In reference to the latter case, any site free of grounded ice is considered to be 'ocean', while other locations are said to be covered by grounded, marine-based ice. In the absence of ice cover, a shoreline is defined wherever $T = SL = 0$.

With this nomenclature in mind, the ocean height may be computed by projecting global sea level defined in eq. (1) onto the region covered by ocean. This projection can be written as

$$S(\theta, \psi, t_j) = SL(\theta, \psi, t_j) \cdot C^*(\theta, \psi, t_j), \tag{3}$$

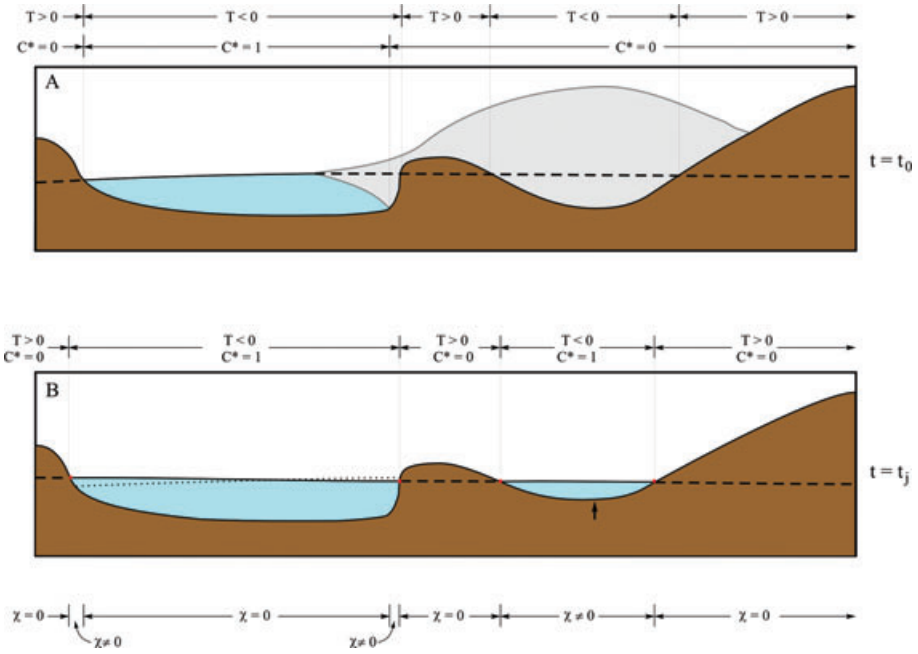

Figure 3. (A) Schematic illustrating the connection between sea level (or topography) and ocean height, following eq. (3). The position of the geoid, G, is given by the top of the open ocean and the dashed line in regions covered by ice or land. The height of the 'solid surface', R, as we define it in the text, is given by the top of the region coloured in brown. Topography is positive (or sea level is negative) where $G < R$ and it is negative (sea level is positive) where $G > R$. Following eq. (4), the ocean function, C^*, is 1 where sea level is positive *and* there is no grounded marine-based ice, and it is zero elsewhere. (B) As in frame (A), except for the situation after all ice (floating and grounded) has melted. The thin dotted line at left on the figure shows the location of the original sea surface (i.e. the sea surface in frame A). At the base of the figure we indicate regions where $\chi \equiv T(t_0)\,[C^*(t_j) - C^*(t_0)]$ is zero or non-zero, where t_0 refers to the situation in frame (A) and t_j is the situation in frame (B). As discussed in the text, χ, which is the second term on the right-hand side of the generalized sea level eq. (13), is non-zero wherever ocean exists at t_j and not t_0, or vice versa. All symbols on the figure suppress the dependence on (θ, ψ, t).

where the ocean function, C^*, is defined by

$$C^*(\theta, \psi, t_j) = \begin{cases} 1 & \text{if } SL(\theta, \psi, t_j) > 0 \text{ and there is no grounded ice} \\ 0 & \text{elsewhere.} \end{cases} \quad (4)$$

The connection between geoid height, G, the radial position of the solid surface, R and sea level, SL, as well as the projection defined by eq. (3), is illustrated in the top frame of Fig. 3. Wherever the geoid (with location given by the top of the water in open ocean regions and by the dashed line elsewhere) lies above the solid surface (the top of the region in brown), irregardless of the presence or absence of ice, the topography is negative (or sea level is positive). Where the geoid lies below the solid surface the topography is positive (sea level is negative). Moreover, the ocean function, C^*, is 1 wherever the topography is negative and there is no grounded ice; this is true over the ocean pictured in the figure, including regions of the ocean that are covered by floating ice. It is important to emphasize that areas in which the ocean function is equal to 1 are, by definition, filled with water from the solid surface up to the sea surface (or covered by an equivalent mass comprised of a combination of water and floating ice).

Changes in the distribution of ice and water, whether in the past or into the future, act to perturb the radial position of the bounding surfaces that define sea level. If we denote these perturbations by ΔG and ΔR, respectively, and the time just prior to the onset of load redistribution by $t = t_0$, then we can express G and R at a later time t_j as

$$\begin{aligned} G(\theta, \psi, t_j) &= G(\theta, \psi, t_0) + \Delta G(\theta, \psi, t_j), \\ R(\theta, \psi, t_j) &= R(\theta, \psi, t_0) + \Delta R(\theta, \psi, t_j). \end{aligned} \quad (5)$$

Using these expressions in eq. (1) yields an analogous decomposition for global sea level

$$SL(\theta, \psi, t_j) = SL(\theta, \psi, t_0) + \Delta SL(\theta, \psi, t_j), \quad (6)$$

where

$$\Delta SL(\theta, \psi, t_j) = \Delta G(\theta, \psi, t_j) - \Delta R(\theta, \psi, t_j). \quad (7)$$

One can write a similar expression for topography. Using (2) in (6) yields

$$T(\theta, \psi, t_j) = T(\theta, \psi, t_0) - \Delta SL(\theta, \psi, t_j). \quad (8)$$

The geoid or sea-surface anomaly, G, is generally separated into spatially varying and spatially uniform components,

$$\Delta G(\theta, \psi, t_j) = \Delta \mathcal{G}(\theta, \psi, t_j) + \frac{\Delta \Phi(t_j)}{g}, \quad (9)$$

where the uniform shift, $\frac{\Delta \Phi(t_j)}{g}$, will be constrained by invoking conservation of mass of the surface load. The decomposition (9) has a straightforward physical interpretation. The sea surface is constrained, in a static sea level theory, to remain an equipotential surface. However, as mass is transferred between ice and ocean reservoirs, and/or the Earth deforms in response to this changing load, the sea surface need not remain on the *same* equipotential surface through time (Dahlen 1976). The first term on the right-hand side of eq. (9) represents the perturbation in the original equipotential surface (i.e. the equipotential surface coincident with sea level at t_0) and the second term is the uniform shift that is associated with a change from one equipotential surface to another.

With this decomposition of the geoid height, we may also define

$$\Delta \mathcal{SL}(\theta, \psi, t_j) = \Delta \mathcal{G}(\theta, \psi, t_j) - \Delta R(\theta, \psi, t_j), \quad (10)$$

and eq. (7) can then be rewritten as

$$\Delta SL(\theta, \psi, t_j) = \Delta \mathcal{SL}(\theta, \psi, t_j) + \frac{\Delta\Phi(t_j)}{g}. \tag{11}$$

Next, we turn to the ocean height. Deriving an expression for the change in ocean height relative to the initial ($t = t_0$) height is more complicated than the above derivations because determining this height requires, following eq. (3), a projection onto the ocean function. If we write, in analogy with eq. (5)

$$S(\theta, \psi, t_j) = S(\theta, \psi, t_0) + \Delta S(\theta, \psi, t_j), \tag{12}$$

then, eqs (2), (3) and (6) yield, after some algebra, the generalized sea level eq. (GSLE) derived by Mitrovica & Milne (2003)

$$\begin{aligned}\Delta S(\theta, \psi, t_j) = {} & \Delta SL(\theta, \psi, t_j) C^*(\theta, \psi, t_j) \\ & - T(\theta, \psi, t_0)[C^*(\theta, \psi, t_j) - C^*(\theta, \psi, t_0)].\end{aligned} \tag{13}$$

The GSLE eq. (13) indicates that the change in ocean height from the onset of loading is comprised of two terms. The first term on the right-hand side is a simple projection of the total change in global sea level onto the ocean function at $t = t_j$ (i.e. from eq. 3, a projection of global sea level onto all marine areas free of grounded ice at $t = t_j$). The second is a term which takes into account changes in geometry of oceans from $t = t_0$ to $t = t_j$. Specifically, this 'correction' term (see Mitrovica & Milne 2003) involves a projection of the initial topography onto a field which is non-zero only in locations in which the ocean geometry has changed during this time interval.

To illustrate these concepts, Fig. 3 shows a rather general case in which an area that includes both floating and grounded marine based ice, as well as land ice (frame A), becomes ice free (frame B). We discussed Fig. 3(A) above. In Fig. 3(B) all areas with negative topography (positive sea level) are oceans (i.e. $C^* = 1$). If we take $t = t_0$ in the frame A and $t = t_j$ in the frame B, then at the bottom of the plot we indicate locations where the second (correction) term on the right-hand side of GSLE eq. (13) is either zero or non-zero. Specifically, this term is non-zero in all regions where the ocean function has changed across the time interval; that is, all locations that accommodate water at $t = t_j$ but not at $t = t_0$ (or vice versa). Thus, this correction term tracks changes in shoreline geometry which can arise from local changes in sea level leading to onlap (e.g. the coast on the far left of the plot) or offlap, or through a combination of these local changes and the disappearance of grounded, marine-based ice (e.g. near the right coast of the ocean at left, and within the marine depression at right.)

Local changes in sea level (i.e. changes in the relative position of the sea surface and solid surface) are governed by the first term on the right-hand side of eq. (13). This term incorporates the gravitational, deformational and rotational changes in sea level driven by the change in the surface mass (ice plus ocean) load. Indeed, it is this term that controls the basic physics of postglacial sea level change that we discussed in Section 1. For example, the movement of water away from the location of a melting ice sheet in response to a loss in gravitational attraction between the ice and water, evident in the fingerprint prediction of Clark & Lingle (1977) (Fig. 2), and also in the change in tilt of the sea surface from Figs 3(A) and (B), would be included in the so-called self-attraction term that would form part of any mathematical expression for $\Delta SL(\theta, \psi, t_j)$. Similarly, we pointed out in Section 1 that standard sea level theories (Farrell & Clark 1976; Clark & Lingle 1977) do not incorporate the inundation of water in regions vacated by the retreat of grounded, marine-based ice, and the expulsion of some of this water as the inundated region viscoelastically rebounds. In the generalized sea level theory, the inundation is included via the second term on the right-hand side of eq. (13), which 'activates' this region as a reservoir for water (note the $\chi \neq 0$ value for the marine depression to the right-hand side of Fig. 3B). However, the physics of water expulsion is captured by the sea level change (or perturbations in the positions of the sea and solid surface) over the inundated region that would be incorporated into any detailed expression for $\Delta SL(\theta, \psi, t_j)$ on the right-hand side of eq. (13).

We must emphasize, however, that the two terms on the right-hand side of the GSLE (13) are not independent of each other: Changes in global sea level, $\Delta SL(\theta, \psi, t_j)$, map into changes in the ocean function $C^*(\theta, \psi, t_j)$ via eq. (4).

It will be useful to rewrite eq. (13) in a slightly modified form. In particular, rather than considering the total change in sea level (or ocean height) from the onset of loading, we can instead consider a change across two successive time steps in the evolution, say from $t = t_{j-1}$ to $t = t_j$. In particular, if the change in ocean height across this shorter time interval is given by

$$\begin{aligned}\delta S(\theta, \psi, t_j) &= S(\theta, \psi, t_j) - S(\theta, \psi, t_{j-1}) \\ &= \Delta S(\theta, \psi, t_j) - \Delta S(\theta, \psi, t_{j-1}),\end{aligned} \tag{14}$$

then eq. (13) can be rewritten as

$$\begin{aligned}\delta S(\theta, \psi, t_j) = {} & -\Delta S(\theta, \psi, t_{j-1}) + \Delta SL(\theta, \psi, t_j) C^*(\theta, \psi, t_j) \\ & - T(\theta, \psi, t_0)[C^*(\theta, \psi, t_j) - C^*(\theta, \psi, t_0)].\end{aligned} \tag{15}$$

Moreover, using the decomposition (11) yields

$$\begin{aligned}\delta S(\theta, \psi, t_j) = {} & -\Delta S(\theta, \psi, t_{j-1}) + \Delta \mathcal{SL}(\theta, \psi, t_j) C^*(\theta, \psi, t_j) \\ & + \frac{\Delta\Phi(t_j)}{g} C^*(\theta, \psi, t_j) \\ & - T(\theta, \psi, t_0)[C^*(\theta, \psi, t_j) - C^*(\theta, \psi, t_0)].\end{aligned} \tag{16}$$

This version of the GSLE is in a form amenable to numerical solution, as we describe in the following section.

2.1 A numerical implementation

For the purpose of brevity it will be useful to rewrite eq. (16) using a notation in which the dependence on the colatitude and east longitude is implicit and the time dependence is indicated by a subscript

$$\delta S_j = -\Delta S_{j-1} + \Delta \mathcal{SL}_j C^*_j + \frac{\Delta\Phi_j}{g} C^*_j - T_0[C^*_j - C^*_0], \tag{17}$$

where we note that only the term $\frac{\Delta\Phi_j}{g}$ is independent of (θ, ψ).

Our GSLE holds for any kind of earth model and may be applied as long as a formalism exists for computing the change in global sea level $\Delta\mathcal{SL}$ given some surface mass (ice plus ocean) loading history. For example, Kendall *et al.* (2005) summarized a complete spectral theory, ultimately based on viscoelastic Love number theory (Peltier 1974), for the case of a rotating, self-gravitating earth model with depth-varying (i.e. 1-D) linear viscoelastic structure. The results described below are based on an implementation of their expressions for $\Delta\mathcal{SL}$, though we adopt a new theory for computing load-induced perturbations in Earth rotation (Mitrovica *et al.* 2005). We emphasize, however, that the same eq. (17) also holds for 3-D earth models of arbitrary complexity, and in this case expressions for $\Delta\mathcal{SL}$ may be generated, for example, using a suite of numerical algorithms that have been designed to treat the 3-D case (Martinec 2000; Wu & van der Wal 2003; Zhong *et al.* 2003; Latychev *et al.* 2005).

In the viscoelastic calculation, the perturbation $\Delta\mathcal{SL}$ is dependent on the complete time history of the surface load and rotation vector. We make this dependence explicit by rewriting eq. (17) in the form

$$\delta S_j = -\Delta S_{j-1} + \Delta\mathcal{SL}_j\left(\underset{0\le m\le j}{\delta I_m}\ ;\ \underset{0\le m<j}{\delta S_m}\ ;\delta S_j;\ \underset{0\le m<j}{\delta\omega_m}\ ;\delta\omega_j\right)C_j^* + \frac{\Delta\Phi_j}{g}C_j^* - T_0[C_j^* - C_0^*], \tag{18}$$

In this expression the history of the surface mass load has been decomposed into increments across two successive time steps of ocean height, δS_m, and ice height, δI_m, which are both functions of (θ, ψ), and an analogous set of increments for perturbations in the rotation vector, $\delta\omega_m$. For reasons that will become clear below, the ocean height and rotation vector increments have been separated into the increment at t_j and all prior increments.

The form of eq. (18) makes clear that the GSLE is an integral equation. That is, the ocean height increment being solved for, δS_j, also appears on the right-hand side of the equation in the expression for $\Delta\mathcal{SL}_j$. This form reflects the fact that changes in the ocean height are governed by the gravitational field of the planet, and that this field is in turn perturbed by ocean height changes. The perturbation arises because of both the direct attraction of the load and the deformation it induces. Other terms on the right-hand side of eq. (18) also depend on the δS_j, albeit implicitly: C_j^* (via eq. 4), $\frac{\Delta\Phi_j}{g}$ (see below), and $\delta\omega_j$ (since the perturbation in the rotation vector will depend on all load increments).

As mentioned above, an expression for $\frac{\Delta\Phi_j}{g}$ may be obtained by invoking conservation of mass of the surface load. Specifically, multiplying both sides of eq. (18) by the density of water, ρ_w, integrating over the surface of the Earth (Ω), and rearranging yields

$$\frac{\Delta\Phi_j}{g} = -\frac{1}{\mathcal{A}_j}\frac{\rho_i}{\rho_w}\iint_\Omega \Delta I_j\,\mathrm{d}\Omega - \frac{1}{\mathcal{A}_j}\iint_\Omega \Delta\mathcal{SL}_j\left(\underset{0\le m\le j}{\delta I_m}\ ;\ \underset{0\le m<j}{\delta S_m}\ ;\delta S_j;\ \underset{0\le m<j}{\delta\omega_m}\ ;\delta\omega_j\right)C_j^*\,\mathrm{d}\Omega + \frac{1}{\mathcal{A}_j}\iint_\Omega T_0[C_j^* - C_0^*]\,\mathrm{d}\Omega, \tag{19}$$

where ρ_i is the density of ice, ΔI_j is the total change in the ice load height from time t_0 to t_j (i.e. the sum of increments δI_m, from $m = 1, j$), and

$$\mathcal{A}_j = \iint_\Omega C_j^*\,\mathrm{d}\Omega. \tag{20}$$

is the area of oceans that is free of grounded ice at t_j.

The system of eqs (18)–(20) may be solved at each time step t_j using an iterative scheme. Specifically, if we use i to denote the iteration counter, then our numerical algorithm is based on the following:

$$\delta S_j^i = -\Delta S_{j-1} + \Delta\mathcal{SL}_j^{i-1}\left(\underset{0\le m\le j}{\delta I_m}\ ;\ \underset{0\le m<j}{\delta S_m}\ ;\delta S_j^{i-1};\ \underset{0\le m<j}{\delta\omega_m}\ ;\delta\omega_j^{i-1}\right)C_j^{*,i-1} + \frac{\Delta\Phi_j^{i-1}}{g}C_j^{*,i-1} - T_0[C_j^{*,i-1} - C_0^*], \tag{21}$$

$$\frac{\Delta\Phi_j^{i-1}}{g} = -\frac{1}{\mathcal{A}_j^{i-1}}\frac{\rho_i}{\rho_w}\iint_\Omega \Delta I_j\,\mathrm{d}\Omega - \frac{1}{\mathcal{A}_j^{i-1}}\iint_\Omega \Delta\mathcal{SL}_j^{i-1}\left(\underset{0\le m\le j}{\delta I_m}\ ;\ \underset{0\le m<j}{\delta S_m}\ ;\delta S_j^{i-1};\ \underset{0\le m<j}{\delta\omega_m}\ ;\delta\omega_j^{i-1}\right)C_j^{*,i-1}\,\mathrm{d}\Omega + \frac{1}{\mathcal{A}_j^{i-1}}\iint_\Omega T_0[C_j^{*,i-1} - C_0]\,\mathrm{d}\Omega, \tag{22}$$

and

$$\mathcal{A}_j^{i-1} = \iint_\Omega C_j^{*,i-1}\,\mathrm{d}\Omega. \tag{23}$$

In these equations, the value of the total ocean height change at the previous time step $t = t_{j-1}$, ΔS_{j-1}, is assumed to be known (i.e. solved for). An initial guess for the ocean height increment δS_j^0 (see below) can then be used, in combination with all ice load increments $\delta I_m (m = 1, j)$ and ocean height and rotation increments before t_j, that is, δS_m and $\delta\omega_m$ for $m = 1, j - 1$, to compute all elements required for the right-hand side of eq. (21): $\delta\omega_j^0$, $\Delta\mathcal{SL}_j^0$, C_j^0, $\mathcal{A}_j^0$, and $\Delta\Phi_j^0$ (in that order). Then, using eq. (21), the next estimate for δS_j^1 may be obtained, and the process repeated until convergence. As a starting guess for δS_j^0 we use the geographically uniform (eustatic) meltwater distribution associated with the ice increment δI_j (i.e. $\delta S_j = -\delta V_j^I \rho_i/\rho_w A_j^o$, where δV_j^I is the change in the volume of ice across the j^{th} time step).

The iteration scheme (21–23) differs significantly from the methodology used in the calculation of ice-age sea level changes (Kendall *et al.* 2005). In our present application, where we are concerned with projections of future sea level change, the initial topography T_0 is simply the present-day topography and it is therefore known. In contrast, in the ice-age problem the initial topography is the topography at the start of the ice-age loading and this is unknown at the onset of the calculation; only the present-day (observed) topography is known. Therefore, in the ice-age application a second 'outer' iteration 'k' loop is applied over the full loading history such that a first guess to the initial topography, $T_0^{k=0}$, is successively refined until the time-stepped numerical scheme yields a present-day topography that has converged to the actual, observed topography (Peltier 1994; Milne *et al.* 1999; Kendall *et al.* 2005).

In the calculations below, we will compare our results to predictions based on the standard sea level equation derived by Farrell & Clark (1976) and adopted by Clark & Lingle (1977). Their derivation assumed that there are no marine-based ice components and that all shorelines remain fixed in time. It also assumes a non-rotating Earth. In this case, the algorithm outlined above simplifies to the following:

$$\delta S_j^i = -\Delta S_{j-1} + \Delta\mathcal{SL}_j^{i-1}\left(\underset{0\le m\le j}{\delta I_m}\ ;\ \underset{0\le m<j}{\delta S_m}\ ;\delta S_j^{i-1}\right)C + \frac{\Delta\Phi_j^{i-1}}{g}C, \tag{24}$$

$$\frac{\Delta\Phi_j^{i-1}}{g} = -\frac{1}{\mathcal{A}}\frac{\rho_i}{\rho_w}\iint_\Omega \Delta I_j\,\mathrm{d}\Omega - \frac{1}{\mathcal{A}}\iint_\Omega \Delta\mathcal{SL}_j^{i-1}\left(\underset{0\le m\le j}{\delta I_m}\ ;\ \underset{0\le m<j}{\delta S_m}\ ;\delta S_j^{i-1}\right)C\,\mathrm{d}\Omega, \tag{25}$$

where C is equal to 1 over the present-day ocean and zero elsewhere, and A is the area of that ocean

$$\mathcal{A} = \iint_\Omega C\,\mathrm{d}\Omega. \tag{26}$$

The sea level algorithm described above will be solved using a so-called pseudo-spectral methodology (Mitrovica & Peltier 1991). In particular, $\Delta\mathcal{SL}_j$ is computed in the spectral (i.e. spherical harmonic) domain, while all projection operations required in the various terms of eqs (21) and (22) are performed in the space domain and then converted into the spectral domain. The switching back and forth between spectral and space domains is motivated by the fact that projections are much more efficiently computed in the space domain (where they are simply multiplications between associated grid elements) than in the spectral domain. Detailed mathematical expressions for $\Delta\mathcal{SL}_j$, based on viscoelastic Love number theory, may be found in Kendall *et al.* (2005), while the complementary theory required to compute perturbations in the rotation vector is given by Mitrovica *et al.* (2005). These spectral calculations are all performed up to spherical harmonic degree and order 512.

3 RESULTS

We will consider two different scenarios for melting from the Antarctic. In the first, we melt the entire WAIS sector of the ice sheet. The total (grounded) volume of the ice sheet corresponds to an eustatic sea level rise of 8.4 m, and an EEV of 5.0 m. In the second, we remove ice only from marine-based sectors of the EAIS (see Fig. 1). This volume, which is taken largely from Wilkes Land, corresponds to a eustatic sea level rise of 18.0 m, and an EEV of 14.2 m. Our ice thickness model for these regions is taken from the EISMINT web site (http://homepages.vub.ac.be/phuybrec/eismint/antarctica.html). The present-day topography, T_0, is given by ETOPO2 (http://www.ngdc.noaa.gov/mgg/fliers/01mgg04.html) with the ice thickness model removed.

Our predictions will be based on an earth model with elastic and density structure taken from the seismic inference PREM (Dziewonski & Anderson 1981). We will begin with predictions of sea level change soon after the collapse of the ice sheets. In this case, we will assume that the time elapsed from the onset of melting to the observation of the sea level change is sufficiently small that no viscous relaxation occurs. This time window depends on the Maxwell time of the Earth, which is unlikely to be less than several hundred years. To investigate the effect of viscous relaxation on these elastic predictions, we end this section with a set of calculations that predict the change in sea level 500 yr after the melting event has ceased. These calculations, in contrast to the elastic predictions, will be sensitive to the adopted radial profile of mantle viscosity, and for this purpose we use a profile that is amongst a class of inferences that has received wide support within the ice-age modelling community (e.g. Lambeck *et al.* 1998; Mitrovica & Forte 2004). The profile is characterized by an elastic lithosphere of thickness 120 km, an upper mantle viscosity of 5×10^{20} Pa s, and a lower mantle viscosity of 5×10^{21} Pa s.

In Figs 4(A) and (B), we show sea level fingerprints, normalized by an EEV of 5 m, for the collapse of the WAIS computed using the full sea level theory (eqs 21–23) and the older theory of Farrell & Clark (1976) (eqs 24–26), respectively. Fig. 4(C) is the difference between these two predictions.

Fig. 4(B) accurately reproduces the fingerprint computed by Clark & Lingle (1977), shown in Fig. 2, despite differences in the adopted elastic earth model (PREM in our case versus 1066B), the geometry of melting (Clark & Lingle 1977, assumed a uniform thinning of the WAIS), and the sea level formalism (Clark & Lingle 1977, solved the sea level equation using a spatial gridding of the Earth's surface which had an effective resolution that was significantly less than our spectral truncation). Fig. 4(B) is characterized by peak values in the north Atlantic and Indian Oceans of 1.19, and a global peak value of 1.25 in the north Pacific Ocean. These values are less than 1 per cent lower than the associated peaks in Fig. 2. Our calculations also show the same tapering down to progressively lower contour values towards the shorelines in the northern oceans. Our results, in contrast to those in Fig. 2, show variations in sea level over both land and water, and these global patterns confirm our earlier physical argument for the tapering. Namely, this trend is due to ocean loading, which causes a downward flexure of the oceans and an upward flexure of the continents.

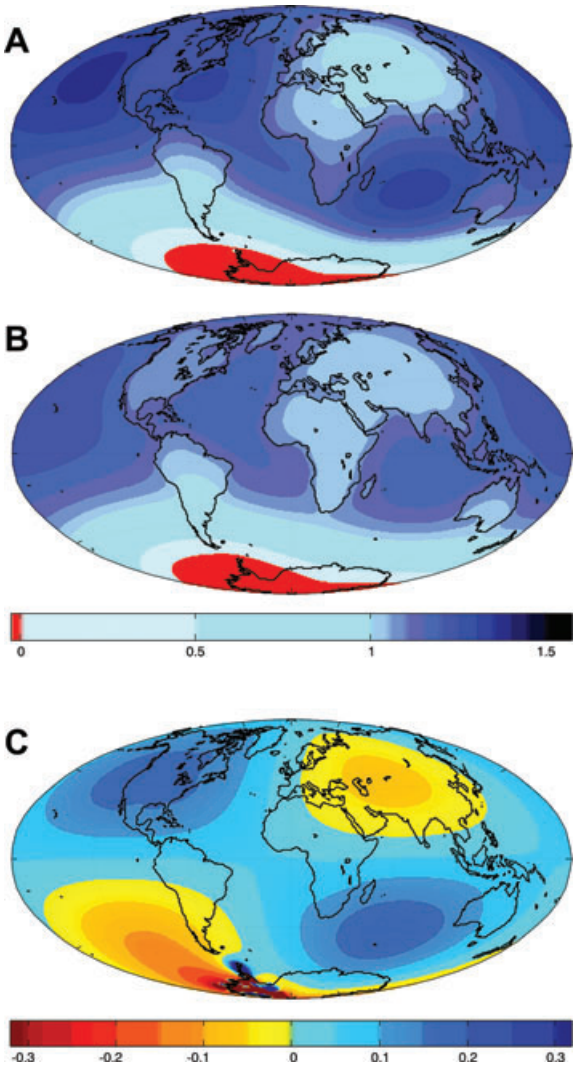

Figure 4. (A) Sea level change in response to the collapse of the WAIS computed using the full sea level theory described by eqs (21)–(23). The total volume of the WAIS is used in the calculation, but the prediction is normalized by the effective eustatic value. (B) As in frame (A), except that the calculations adopt an older sea level theory (see eqs 24–26) which assumes a non-rotating Earth, no marine-based ice and shorelines that remain fixed (to the present-day geometry) with time. In this calculation only an amount of ice with a volume that matches the effective eustatic sea level rise for the ice model in frame (A) (5.0 m; see text) is removed from the system. (C) The difference between predictions generated using the new and old sea level theories (frame A minus B). The figure is modified from Mitrovica *et al.* (2009).

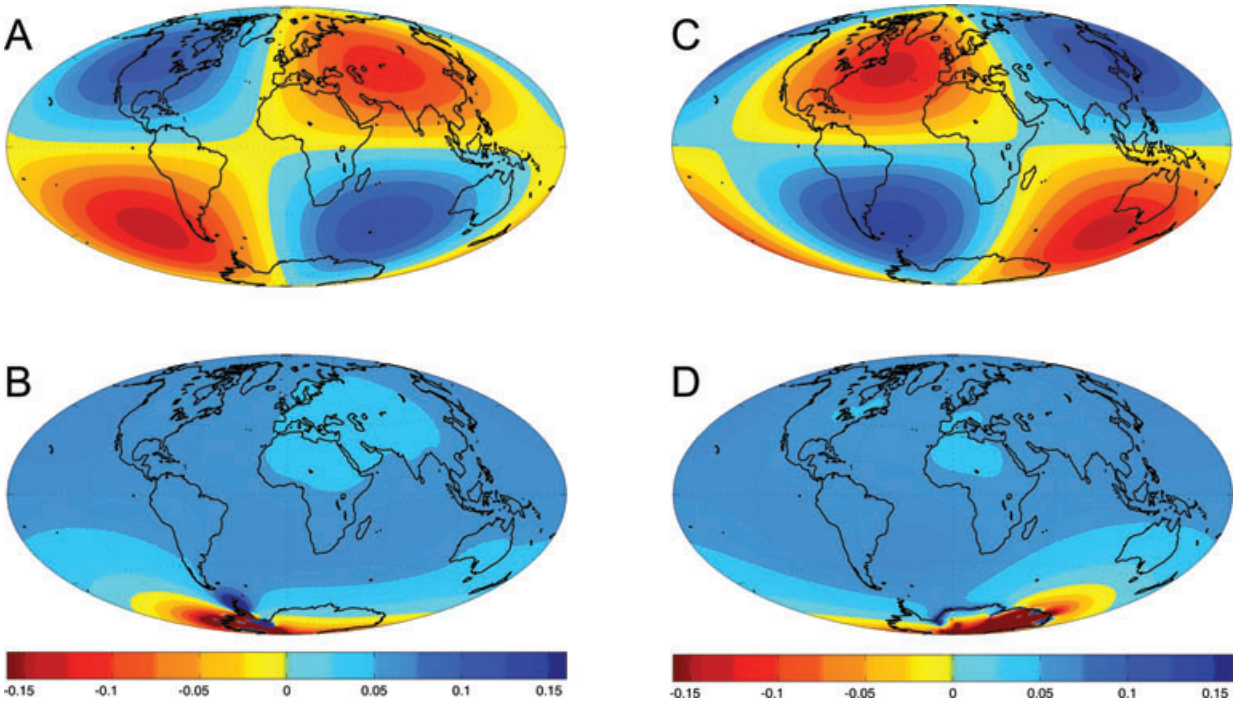

Figure 5. (A and B) Decomposition of the difference between predictions of sea level change due to the collapse of the WAIS based on the new and old sea level theories (i.e. Fig. 4C). Specifically, the difference is decomposed into contributions associated with (A) feedback due to Earth rotation and (B) the expulsion of water from uplifting and flooded marine-based sectors of the now-vanished ice sheet. (C) and (D), as in (A) and (B), except for the case of the EAIS and a decomposition of the difference plot shown in Fig. 9(C).

A comparison between Figs 4(A) and (B) indicates that the new sea level theory described in the last section yields a far-field signal that is characterized by significantly enhanced sea level rise relative to the theory adopted by Clark & Lingle (1977). The peaks in the north Atlantic and north Pacific ocean reach 1.32 and 1.37, respectively, and both have migrated closer to the coastlines of North America, while the peak in the Indian Ocean is 1.33. The difference plot (Fig. 4C) indicates that the largest enhancements occur on the coasts of the United States, and in particular the west coast; in these regions, the new theory predicts a normalized sea level rise $\sim$0.15 higher than the older theory, or 0.8 m for an EEV of 5 m. A similar enhancement occurs over the southern Indian Ocean.

The pattern evident in Fig. 4(C) is strongly suggestive of a dominant contribution from rotational effects, which are characterized by the same 'quadrential' sea level geometry (e.g. Mound & Mitrovica 1998). We explore this issue in detail in Fig. 5(A), where we isolate the contribution to the signal from rotational feedback. The figure shows the difference between a prediction based on the old theory (Fig. 4B) and a second prediction, also based on the old theory, in which we turn on the contribution to changes in the sea level from perturbations in Earth rotation. In addition, Fig. 5(B) shows the difference between a calculations based on the new theory (Fig. 4A) and the old theory where we once again incorporate rotational effects; that is, the figure plots the part of the discrepancy between the old and the new theory that is not explained by rotational feedback.

The physics of rotational feedback is outlined in Fig. 6 and the associated caption. A reorientation of the rotation pole is accompanied by a rise in sea level in quadrants that the local pole (either the north pole in the northern hemisphere or the south pole in the southern hemisphere) is moving away from and a fall in sea level in antipodal quadrants. The maximum sea level signal will be 45° from the poles. In our calculations, the collapse of the WAIS leads to a shift in the rotation pole of 92 m per metre of effective eustatic sea level rise (or $\sim$0.46 km for an EEV of 5 m); the direction of the polar wander is such that the South Pole moves towards the West Antarctic (253°E longitude) and the north pole moves towards India (73° E). Accordingly, the maximum positive sea level rise due to rotational feedback occurs over North America and the Indian Ocean (while the antipodal regions of sea level fall occur in Asia and the southeast Pacific). This positive signal, which reaches a magnitude of 0.11 (or $\sim$0.6 m for an EEV of 5 m), is clearly responsible for a large part of the enhanced sea level rise over North America and the Indian Ocean. Moreover, the contribution in Fig. 5(A) is also responsible for the fact that the peak sea level predictions obtained using the new theory (Fig. 4A) occur closer to the U.S. coastlines than the calculations generated using the old theory (Fig. 4B).

The relatively large rotational feedback signal in response to the collapse of the WAIS may be surprising given that the location of the Antarctic, close to the pole, would seem to make any loading from the region a somewhat inefficient mechanism for driving polar wander. However, the centre of mass of the West Antarctic is $\sim$10° from the south pole, and this displacement is clearly sufficient to drive a significant reorientation of the pole.

The second contribution that distinguishes the new predictions from the old, which is shown in Fig. 5(B), is less geographically variable in the far-field of the West Antarctic. This contribution is primarily due to water being pushed out of the marine-based sector of the exposed West Antarctic as this region rebounds elastically in response to the melting. To investigate this issue, we replot, in Fig. 7(A), the total sea level change driven by WAIS collapse (Fig. 4A) in a new projection centred on the South Pole. The figure shows that there is a significant fall in sea level within the West Antarctic, reaching $\sim$17 times the amplitude of the EEV, driven by

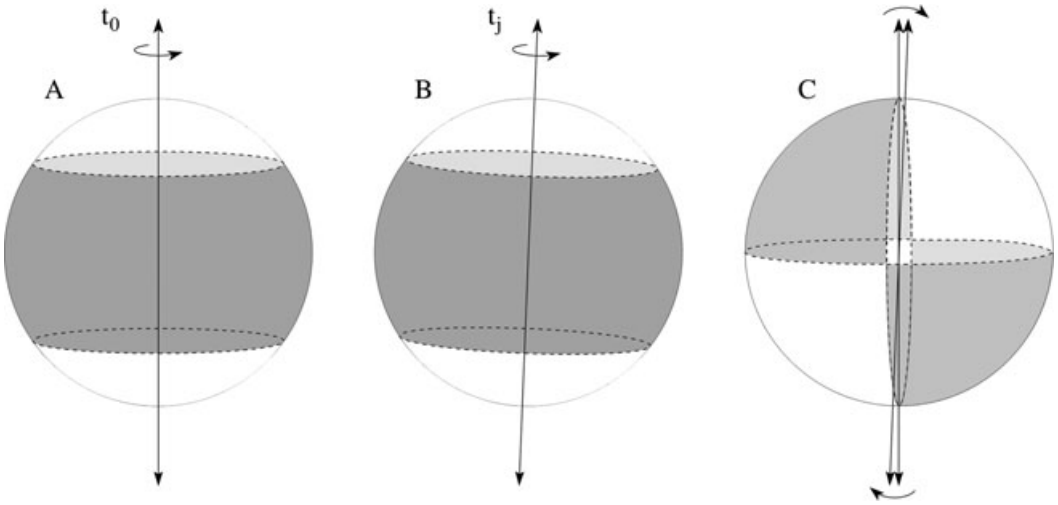

Figure 6. Schematic illustrating the geometry of the rotational feedback contribution to sea level. (A) and (B) show the orientation of the centrifugal potential for an earth model prior to the melting event (t_0) and some time after the melting event (t_j), respectively. From t_0 to t_j the rotation pole, which was initially vertical, is assumed to have moved in a clockwise direction (compare frames A and B) relative to the solid surface of the planet. (C) shows the difference in centrifugal potential between the two frames (B minus A) associated with the true polar wander event. The geometry in frame (A) is given by the spherical harmonic degree two and order zero harmonic, while the perturbation in this potential, the so-called rotational driving potential, has a spherical harmonic degree two and order one (quadrential) geometry (frame C). The orientation in (C) is such that the driving potential is positive in quadrants that the local pole (N in the north and S in the south) is moving away from (shaded regions) and negative in the antipodal quadrants. The driving potential is zero along two great circles; the first is along the equator, and the second is perpendicular to both the equator and the great circle that defines the pole path. The driving potential is at a maximum 45° from the pole. The rotational feedback sea level signal has essentially the same geometry as the driving potential shown in (C), although the former is perturbed by loading effects.

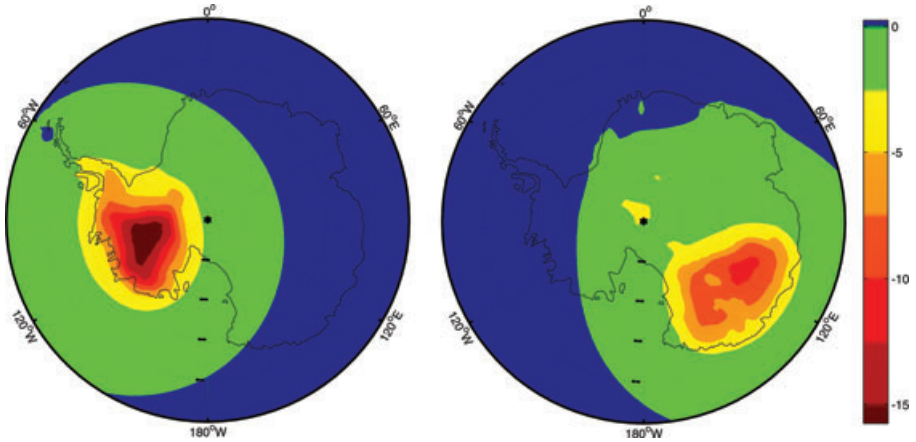

Figure 7. (A) A prediction of the change in sea level over the south pole following the collapse of the WAIS. The figure is a different projection of the results plotted in Fig. 4(A). (B) As in (A), except for the case of a collapse of the EAIS (a different projection of Fig. 9A).

the radial uplift of the crust and the loss of gravitational attraction towards the now-vanished WAIS. In any marine-based sectors of the West Antarctic (i.e. in regions covered by water) this sea level fall means that water is being pushed out of the region. The expulsion of water from these marine-based sectors is responsible for a normalized sea level rise of up to ∼0.07 (or ∼0.3 m for an EEV of 5 m).

Over North America and the Indian Ocean the rotational feedback and water expulsion signals constructively interfere and the new sea level theory predicts a (normalized) enhancement of the sea level rise relative to old calculations (Clark & Lingle 1977). Over the southeast Pacific and Asia, where the two effects destructively interfere, the new theory predicts a somewhat smaller sea level signal than the old calculation (Fig. 4C).

The normalized fingerprint in Fig. 4(A) is identical to the calculation published in our recent note (Mitrovica *et al.* 2009). An independent prediction of the fingerprint of WAIS collapse was also recently described by Bamber *et al.* (2009). Their projection of the sea level change showed a more muted amplification over the regions offshore of the U.S. west coast and in the Indian Ocean (amplitudes ∼25 per cent above the EEV). A detailed comparison of the differences in the two calculations is beyond the scope of the present paper and will be the subject of future work. However, one difference between the predictions is the adoption, by Bamber *et al.* (2009), of an incompressible elastic Earth rheology. We repeated our calculations using this simplification and the resulting normalized sea level fingerprint is shown in Fig. 8(A). Fig. 8(B) shows the difference between the compressible and incompressible calculations. The assumption of incompressibility reduces the solid Earth deformational response to the deglaciation (most notably at spherical harmonic degree two) and this acts, in turn, to reduce the amplitude of the sea level fingerprint. The assumption plays a role

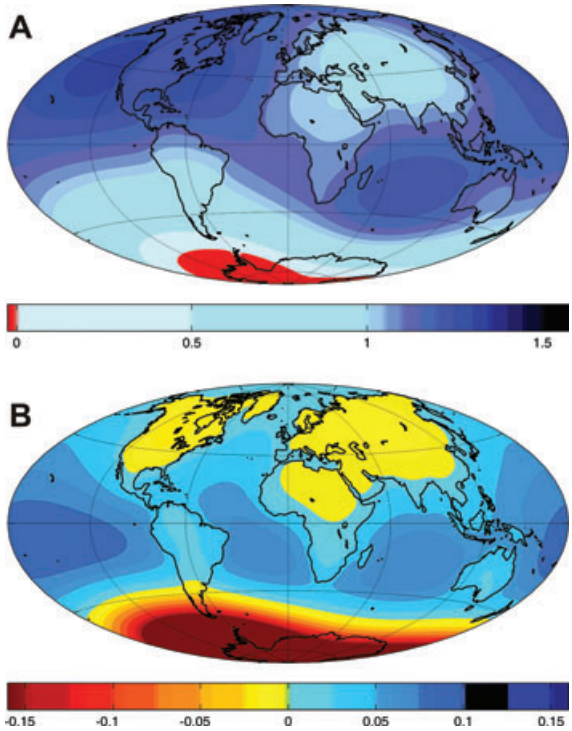

Figure 8. (A) Sea level change in response to the collapse of the WAIS computed as in Fig. 4(A) with the exception that the elastic response of the Earth is assumed to be incompressible. (B) The difference between the compressible and incompressible predictions of the normalized sea level fingerprint of WAIS collapse (i.e. Figs 4A minus 8A).

in the discrepancy between the published results, and we conclude that accurate predictions of sea level projections should adopt a compressible elastic rheology.

Next, we turn to the case of the collapse of marine-based sectors of the East Antarctic Ice Sheet (EEV = 14.2 m). Figs 9(A) and (B) are predictions of the sea level change just after this collapse based on the new sea level theory (eqs 21–23) and the older theory adopted by Farrell & Clark (1976) (eqs 24–26), respectively. The difference between the two is shown in Fig. 9(C). The normalized sea level rise is increased by ∼0.2 in the northwest Pacific and the southwest Atlantic (which translates to a difference of ∼3 m if we use an EEV of 14.2 m), while it is reduced by ∼0.08 in the north Atlantic.

The origin of these differences is evident in Figs 5(C) and (D), where we once again decompose the signal into contributions from rotational feedback (Fig. 6) and water expulsion from the marine-sectors of the melting ice complex (Fig. 7B). As before, the expulsion yields a sea level rise over the far-field of the now-vanished ice sheet. The normalized amplitude of this signal is ∼0.07. A far more significant difference between the WAIS and EAIS scenarios is the orientation of the rotational feedback signal (compare Figs 5A and C). Melting of the marine sectors of the EAIS leads to a displacement of the rotation pole of ∼102 m per metre of EEV. The direction of the displacement is such that the south pole moves towards Wilkes Land in the East Antarctic (specifically, along ∼131°E longitude) and the north pole moves along ∼49°W longitude, or roughly towards Newfoundland. The resulting feedback signal is a sea level fall over the north Atlantic and the south Indian Ocean and a sea level rise in antipodal quadrants (Fig. 5C), each with a (normalized) magnitude of 0.13. (This value is slightly higher than the amplitude in Fig. 5(A) because marine sectors of the EAIS have a centre of mass that is slightly more distant from the south pole than the centre

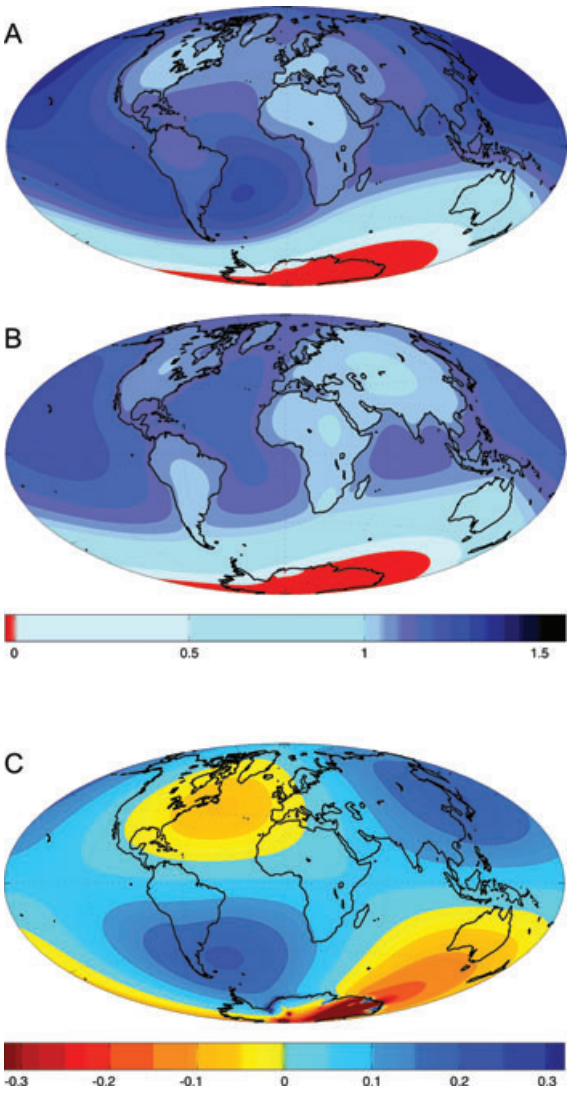

Figure 9. As in Fig. 4, except for predictions based on a scenario where marine-based sectors of the EAIS are removed. In this case, the effective eustatic value used in the normalization of the results is 14.2 m. A decomposition of the difference plot (C) into contributions from rotational feedback and water expulsion from the uplifting marine-based sector of the EAIS is shown in Figs 5(C) and (D), respectively.

of mass of the WAIS.) Thus, for this melting scenario our new sea level theory predicts a significantly enhanced sea level rise over the north Pacific and the south Atlantic, where rotational feedback and expulsion constructively interfere, and a reduced sea level rise over the north Atlantic, where the interference is destructive and the rotational effect dominates, relative to the old theory.

We note that polar motion driven by melting from the WAIS and marine sectors of the EAIS are roughly in opposite directions. As a consequence, if both melting scenarios were active and with similar EEVs then the total rotational feedback (the sum of Figs 5A and C) would have a significantly smaller amplitude than the individual feedback signals. In other words, in this case the common view that melting from the Antarctic ice sheet would lead to relatively little net true polar wander (and sea level feedback signal) would be correct.

Our focus, to this point, has been on the short-term, elastic response to rapid melting from either the WAIS or the EAIS sectors

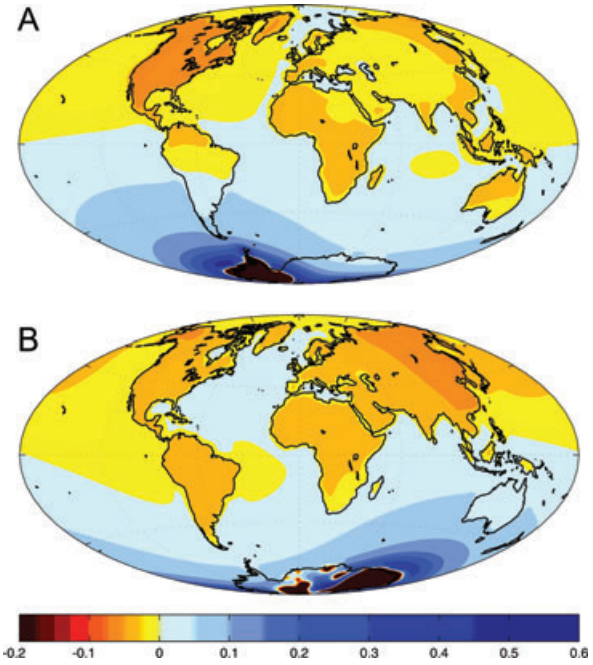

Figure 10. (A) Change in sea level, normalized by the effective eustatic value, in the 500 year period following the 'elastic' sea level fingerprint associated with WAIS melting shown in Fig. 4(A). The total sea level change at this time is the sum of the two maps. (B) As in frame (A), except for the EAIS melting scenario considered in Fig. 9(A). The calculations in this figure, in contrast to those shown in Figs 4 and 9, are sensitive to the adopted radial profile of mantle viscosity. The profile we adopt is specified in detail in the text.

of Antarctica. In Fig. 10, we show predictions of the change in sea level over a 500 yr time window following this immediate elastic response. The calculations adopt the radial profile of mantle viscosity discussed above (with an upper mantle viscosity of 5×10^{20} Pa s, and a lower mantle viscosity of 5×10^{21} Pa s). As the system evolves forward from the short term response, the ongoing uplift of marine-based sectors of the vanished ice sheet would lead to a continued expulsion of water. However, the physics of viscoelastic adjustment is such that the associated rise in sea level is largely limited to areas just outside the zone of melting. Specifically, the subsidence of the 'peripheral bulge' produces a ring of sea level rise that accommodates the water migration due to expulsion. In the far-field oceans the change in sea level is more moderate, and the small trend from ocean to continent regions reflects both ocean loading effects (which tend to deflect the continents upward) and a superimposed rotational feedback. In any event, we conclude that the elastic fingerprints patterns described above (Figs 4 and 9) will not be altered significantly in the far-field of Antarctica in the centuries following any collapse of the ice sheets.

4 FINAL REMARKS

The goal of this paper has been to provide updated predictions of the sea level change that would follow any future collapse of various marine-based sectors of the Antarctic ice sheet. As we have shown, an accurate prediction of this change, and in particular its geographic variation, requires a sea level theory that includes self-gravitation of the surface mass load, inundation and subsequent adjustment of marine-based sectors of the ice sheet, and the feedback into sea level of contemporaneous perturbations in the Earth's rotation.

We have been motivated, in part, by recent discussions of sea level projections associated with the disappearance of the WAIS. As an example, chapter 10 of the IPCC report cites a sea level rise of 5 m in this case (IPCC 2007), which is an estimate of the uniform rise in sea level within the global oceans after all depressions in marine sectors of the West Antarctic have been filled to sea level. We have coined the term 'EEV' for this rise, to distinguish it from the eustatic value (∼8 m) associated with the total volume of the WAIS. It has been important to note that quoting the EEV ignores a prediction, now 30 years old, that demonstrated the significant geographic variation in sea level that would follow the melting event (Clark & Lingle 1977). Specifically, Clark & Lingle (1977) showed that load self-gravitation, and the associated adjustment of the crust, would lead to a dramatic migration of water from the near field to the far field of the melt zone; the net effect would be a sea level fall in the vicinity of the melting, and a sea level rise about 20 per cent greater than the EEV in the far field. We have shown that the expulsion of water from marine-based sectors of the WAIS and rotational feedback are capable of increasing this enhancement relative to the EEV by about a factor of two in regions where the two processes constructively interfere (e.g. the coastlines of North America and the Indian Ocean). In locations where the two processes destructively interfere, the net effect is a reduction in sea level relative to predictions based on the 'old' theory adopted by Clark & Lingle (1977) (Fig. 4).

Similar conclusions can be drawn from our calculation in which all marine sectors of the EAIS disappeared (Fig. 9). In this case, over the northwest Pacific and the south Atlantic, rotational feedback and water expulsion act in tandem to double the enhancement of sea level rise (relative to the EEV) predicted using the old theory of Clark & Lingle (1977). In contrast, in the north Atlantic, where the two processes are of opposite sign, the net prediction based on our new theory is nearly equal to the results based on the old theory.

The importance of water expulsion and rotation can be further illustrated by considering results for specific geographic sites, rather than simply comparing peak predictions based on the new and old theories (since these peaks may not be located at the same place). In Table 1, we list normalized sea level predictions for a set of 18 sites obtained using the new and old theories. The table includes results

Table 1. Normalized sea level predictions obtained using the new and old theories.

Site	WAIS		EAIS	
	New theory	Old theory	New theory	Old theory
Vancouver	1.26	1.10	1.15	1.11
Portland	1.26	1.11	1.07	1.11
San Francisco	1.31	1.14	1.19	1.14
Los Angeles	1.29	1.13	1.17	1.13
Boston	1.27	1.12	1.08	1.11
New York	1.26	1.11	1.07	1.11
Washington	1.25	1.09	1.07	1.10
Savannah	1.26	1.11	1.12	1.11
Miami	1.29	1.14	1.16	1.15
Rio de Janeiro	1.02	1.01	1.29	1.11
Buenos Aires	0.82	0.85	1.28	1.06
Lima	1.05	1.09	1.25	1.12
Santiago	0.80	0.85	1.26	1.07
London	1.11	1.09	1.09	1.09
Lisbon	1.15	1.11	1.09	1.11
Chennai	1.11	1.11	1.23	1.10
Melbourne	1.07	0.99	0.60	0.68
Tokyo	1.16	1.16	1.38	1.17

for both of the melting scenarios considered in this paper; namely, melting of the entire WAIS and all marine sectors of the EAIS. In the case of sites along the U.S. coast and WAIS collapse, the old theory predicts a normalized sea level change of ∼1.1, or a 10 per cent enhancement above the EEV. In contrast, the new theory increases this enhancement by a factor of 2.5, or ∼0.7 m of additional sea level rise if we adopt an EEV of 5 m. In the case of the EAIS scenario, the old theory yields a sea level change in southern South America (e.g. Santiago, Buenos Aires) of ∼6–7 per cent above the EEV, while this enhancement is increased by a factor of four (to 26–28 per cent) when the new theory is adopted. A similar (∼20 per cent) increase in the normalized prediction is also evident in Japan between the old and new theories.

We conclude that at many locations the rotational feedback and water expulsion contribute significantly more than load self-attraction, which has been the focus of many previous discussions of sea level fingerprints, including Clark & Lingle (1977)'s estimate of sea level change following melting from the WAIS. In this regard, we note that while rotational feedback would be active throughout the melting event, water expulsion would only be activated once marine-based sectors of ice disappear and inundation begins.

ACKNOWLEDGMENTS

We thank two anonymous reviewers for their constructive comments. The authors acknowledge funding from Harvard University (NG, JXM), NSERC (NG, JXM), the Canadian Institute for Advanced Research (JXM), NERC's Oceans 2025 program (MET) and NSF (PUC).

REFERENCES

Bamber, J.L., Riva, R.E.M., Vermeersen, B.L.A. & LeBrocq, A.M., 2009. Reassessment of the potential sea-level rise from a collapse of the West Antarctic Ice Sheet, *Science,* **324,** 901–903.

Clark, J.A. & Lingle, C.S., 1977. Future sea-level changes due to West Antarctic ice sheet fluctuations, *Nature,* **269,** 206–209.

Clark, J.A. & Primus, J.A., 1987. Sea-level changes resulting from future retreat of ice sheets: an effect of CO_2 warming of the climate, in *Sea-Level Changes,* pp. 356–370, eds Tooley, M.J. & Shennan, I., Institute of British Geographers, London, United Kingdom.

Clark, P.U., Mitrovica, J.X., Milne, G.A. & Tamisiea, M.E., 2002. Sea level fingerprinting as a direct test for the source of global meltwater pulse IA, *Science,* **295,** 2438–2441.

Conrad, C. & Hager, B.H., 1997. Spatial variations in the rate of sea level rise caused by present-day melting of glaciers and ice sheets, *Geophys. Res. Lett.,* **24,** 1503–1506.

Dahlen, F.A., 1976. The passive influence of the oceans upon the rotation of the Earth, *Geophys. J. R. astr. Soc.,* **46,** 363–406.

Dziewonski, A.M. & Anderson, D.L., 1981. Preliminary reference Earth model (PREM), *Phys. Earth planet. Inter.,* **25,** 297–356.

Farrell, W.E. & Clark, J.A., 1976. On postglacial sea level, *Geophys. J. R. astr. Soc.,* **46,** 647–667.

IPCC: Climate Change 2007: The Physical Science Basis. Contribution of Working Group I to the Fourth Assessment Report of the Intergovernmental Panel on Climate Change [Solomon, S., Qin, D., Manning, M., Chen, Z., Marquis, M., Averyt, K.B., Tignor, M. & Miller, H.L. (eds.)]. Cambridge University Press, Cambridge, United Kingdom and New York, NY, USA, 966 pp.

Johnston, P., 1993. The effect of spatially non-uniform water loads on predictions of sea level change, *Geophys. J. Int.,* **114,** 615–634.

Kendall, R.A., Mitrovica, J.X. & Milne, G.A., 2005. On post-glacial sea level—II. Numerical formulation and comparative results on spherically symmetric models, *Geophys. J. Int.,* **161,** 679–706.

Kendall, R.A, Mitrovica, J.X., Milne, G.A., Törnqvist, T.E. & Li, Y., 2008. The sea-level fingerprint of the 8.2 ka climate event, *Geology,* **36,** 423–426.

Lambeck, K., Smither, C. & Johnston, P., 1998. Sea-level change, glacial rebound and mantle viscosity for northern Europe, *Geophys. J. Int.,* **134,** 102–144.

Latychev, K., Mitrovica, J.X., Tromp, J., Tamisiea, M.E., Komatitsch, D. & Christara, C., 2004. Glacial isostatic adjustment on 3-D earth models: a new finite-element formulation, *Geophys. J. Int.,* **161,** 421–444.

Martinec, Z., 2000. Spectral–finite element approach to three-dimensional viscoelastic relaxation in a spherical earth, *Geophys. J. Int.,* **142,** 117–141.

Mercer, J.H., 1978. West Antarctic ice sheet and CO_2 greenhouse effect: a threat of disaster, *Nature,* **271,** 321–325.

Milne, G.A., 1998. Refining models of the glacial isostatic adjustment process, *PhD thesis*, University of Toronto, Toronto.

Milne, G.A. & Mitrovica, J.X., 1996. Postglacial sea-level change on a rotating Earth: first results from a gravitationally self-consistent sea-level equation, *Geophys. J. Int.,* **126,** F13–F20.

Milne, G.A. & Mitrovica, J.X., 1998. Postglacial sea-level change on a rotating Earth, *Geophys. J. Int.,* **133,** 1–10.

Milne, G.A., Mitrovica, J.X. & Davis, J.L., 1999. Near-field hydro-isostasy: the implementation of a revised sea-level equation, *Geophys. J. Int.,* **139,** 464–482.

Mitrovica, J.X., 2003. Recent controversies in predicting post-glacial sea-level change: a viewpoint, *Quat. Sci. Rev.,* **22,** 127–133.

Mitrovica, J.X. & Forte, A.M., 2004. A new inference of mantle viscosity based upon a joint inversion of convection and glacial isostatic adjustment data, *Earth Planet. Sci. Lett.,* **225,** 177–189.

Mitrovica, J.X. & Milne, G.A., 2003. On post-glacial sea level: I. General theory, *Geophys. J. Int.,* **154,** 253–267.

Mitrovica, J.X., Gomez, N. & Clark, P.U., 2009. The sea-level fingerprint of West Antarctic collapse, *Science,* **323,** 753.

Mitrovica, J.X. & Peltier, W.R., 1991. On postglacial geoid subsidence over the equatorial oceans, *J. geophys. Res.,* **96,** 20 053–20 071.

Mitrovica, J.X., Tamisiea, M.E., Davis, J.L. & Milne, G.A., 2001. Polar ice mass variations and the geometry of global sea level change, *Nature,* **409,** 1026–1029.

Mitrovica, J.X., Wahr, J., Matsuyama, I. & Paulson A., 2005. The rotational stability of an ice age Earth, *Geophys. J. Int.,* **161,** 491–506.

Mound, J.E. & Mitrovica, J.X., 1998. True polar wander as a mechanism for second-order sea-level variations, *Science,* **279,** 534–537.

Nakiboglu, S.M. & Lambeck, K., 1991. Secular sea-level change, in *Glacial Isostasy, Sea-Level and Mantle Rheology,* pp. 237–258, eds Sabadini, R., Lambeck, K. & Boschi, E., Kluwer Academic Publishers, Dordrecht, The Netherlands.

Peltier, W.R., 1974. The impulse response of a Maxwell Earth, *Rev. Geophys.,* **12,** 649–669.

Peltier, W.R., 1994. Ice age paleotopgraphy, *Science,* **265,** 195–201.

Peltier, W.R., 1998. Postglacial variations in the level of the sea: implications for climate dynamics and solid-Earth geophysics, *Rev. Geophys.,* **36,** 603–689.

Plag, H.-P. & Jüttner, H.U., 2001. Inversion of global tide gauge data for present-day ice load changes, in *Proceedings of the Second International Symposium on Environmental Research in the Arctic and Fifth Ny-Alesund Scientific Seminar, Mem. Nat. Inst. Polar Res.,* **54,** 301–318.

Tamisiea, M.E., Mitrovica, J.X., Milne, G.A. & Davis, J.L., 2001. Global geoid and sea level changes due to present-day ice mass fluctuations, *J. geophys. Res.,* **106,** 30 849–30 863.

Woodward, R.S., 1888. On the form and position of mean sea level, *United States Geol. Survey Bull.,* **48,** 87–170.

Wu, P. & van der Wal, W., 2003. Postglacial sea levels on a spherical, self-gravitating viscoelastic Earth: effects of lateral viscosity variations in the upper mantle on the inference of viscosity contrasts in the lower mantle, *Earth planet. Sci. Lett.,* **211,** 57–68.

Zhong, S., Paulson, A. & Wahr, J., 2003. Three-dimensional finite element modelling of Earth's viscoelastic deformation: effects of lateral variations in lithospheric thickness, *Geophys. J. Int.,* **155,** 679–695.